



## Comparison of the effects of MoSi<sub>2</sub> and CrSi<sub>2</sub> on sintering and properties of titanium diboride (TiB<sub>2</sub>)

Agnieszka Gubernat, Łukasz Zych, Dariusz Zientara, Kamil Kornaus\*, Sebastian Komarek, Natalia Skorupa, Zbigniew Pędzich

AGH-University of Science and Technology, Faculty of Materials Science and Ceramics, Mickiewicza 30 av, 30-059 Krakow, Poland

Received 23 June 2023; Received in revised form 6 November 2023; Accepted 14 November 2023

### Abstract

Titanium diboride (TiB<sub>2</sub>) is a typical material classified as structural ceramics. However, sintering of TiB<sub>2</sub> ceramics is difficult mainly because of a significant fraction of covalent bonds in the structure. In order to obtain dense TiB<sub>2</sub> ceramics various additives are used to improve its sinterability. In this study, we investigated effects of MoSi<sub>2</sub> and CrSi<sub>2</sub> additions on sintering and properties of TiB<sub>2</sub> prepared by hot-pressing technique. The sintered materials were characterized in terms of apparent density and microstructure. Their mechanical properties (bending strength, Vickers hardness and fracture toughness) and oxidation resistance were determined. It was found that the obtained composites are characterized by high density and microstructure characteristic for cermets (TiB<sub>2</sub>-MoSi<sub>2</sub>). The activators used for sintering did not deteriorate mechanical properties of TiB<sub>2</sub> sintered bodies. The oxidation resistance of the polycrystals with chromium silicide addition reaches 1400 °C. Based on the carried-out studies, CrSi<sub>2</sub> was found to be a promising sintering additive.

**Keywords:** borides, hot pressing, hardness, oxidation resistance, microstructure

### I. Introduction

Titanium boride (TiB<sub>2</sub>), due to the combination of favourable performances, such as low density (4.52 g/cm<sup>3</sup>), high melting point (3225 °C) and high thermal conductivity (60–120 W/(m·K)), with good mechanical properties, i.e. Vickers hardness (20–30 GPa), Young's modulus (400–500 GPa), bending strength (300–450 MPa) and fracture toughness (4–6 MPa·m<sup>0.5</sup>) is an excellent candidate for many high-temperature applications [1–5]. However, the production of dense TiB<sub>2</sub> polycrystals is a major problem which results from strong covalent bonds dominating its structure [1–3]. Both physical and chemical activation of the sintering process can be used to improve TiB<sub>2</sub> sinterability.

Data on the sintering of TiB<sub>2</sub> ceramics and applied densification-enhancing additives can be found in the literature. There are many papers on the role of metallic binders in TiB<sub>2</sub> densification. Ferber *et al.* [6] used up to 10 wt.% of Ni and produced a polycrystals with

a relative density higher than 99 %TD by hot pressing at 1425 °C. On the other hand, Kang *et al.* [2,7] observed that the simultaneous addition of 0.5 wt.% Fe and 0.5 wt.% Cr increases the densification of TiB<sub>2</sub> in the temperature range 1800–1900 °C, but the addition of Fe activates discontinuous grain growth, thus worsening the density of the sintered body. The situation changes when B<sub>4</sub>C is introduced along with Fe addition [2,8]. A relative density close to 95 %TD is then achieved. In the case of metallic sintering activators, a significant deterioration of properties of the polycrystals is observed with increasing temperature [2,6,7], so non-metallic additives are favoured. Various non-metallic additives such as: AlN [9], ZrO<sub>2</sub> [10–16], SiC [12,14,16–18], Si<sub>3</sub>N<sub>4</sub> [19], CrB<sub>2</sub> [19,20], B<sub>4</sub>C [8,21], TaC [22], TiC [22,23], WC [22], TiN [22], ZrN [22], ZrB<sub>2</sub> [22] as well as MoSi<sub>2</sub>, CrSi<sub>2</sub> and TiSi<sub>2</sub> [1–5,24–27] have been used for TiB<sub>2</sub> sintering activation. Torizuka *et al.* [12,16] observed that hot isostatic pressing (HIP) of TiB<sub>2</sub> with ZrO<sub>2</sub> and SiC additives produces a liquid phase of (Ti,Zr)<sub>5</sub>Si<sub>3</sub> and also small amounts of a liquid phase composed of amorphous SiO<sub>2</sub>. Watanabe and Shoubu [28] identified the formation of a solid so-

\* Corresponding authors: tel: +48 577772640,  
e-mail: [kornaus@agh.edu.pl](mailto:kornaus@agh.edu.pl)

lution of  $(\text{Ti,Zr})\text{B}_2$  in hot-pressed  $\text{TiB}_2$  - 30 wt.%  $\text{ZrO}_2$  composites. Also, Telle *et al.* [10] observed formation of solid solution of  $(\text{Zr,Ti})\text{O}_2$  and  $(\text{Ti,Zr})\text{B}_2$  when  $\text{ZrO}_2$  addition was 25 wt.%. The work of Murata *et al.* [22] reported the effectiveness of TaC and TaN additives in  $\text{TiB}_2$  densification. In this case, the formation of solid solutions of  $(\text{Ti,Ta})\text{B}_2$  and  $(\text{Ta,Ti})(\text{C,N})$  was observed during hot pressing at 2100 °C. In contrast, in the case of 20 wt.% AlN addition, the formation of phases such as BN, TiN and  $\text{Al}_2\text{O}_3$  was observed during hot pressing at 1800 °C [9]. The addition of  $\text{Si}_3\text{N}_4$  was also used, which was found to have a beneficial effect on the densification and suppression of grain growth during sintering at 1800 °C [19]. Sintering of  $\text{TiB}_2$  with silicides is activated due to the presence of a liquid phase [1–5,24,27]. The reactive liquid phase consists mainly of  $\text{TiSi}_2$ , which melts around 1500 °C [4] and is formed during the reaction of silicides with  $\text{TiB}_2$ .

In this study, an attempt to produce dense polycrystals based on  $\text{TiB}_2$  was made. The chromium ( $\text{CrSi}_2$ ) and molybdenum ( $\text{MoSi}_2$ ) silicides were used as sintering-activating additives. Each additive was introduced in an amount of 10 wt.%. It is worth mentioning that, among the various high-temperature intermetallic additives  $\text{MoSi}_2$  has high thermal conductivity (53 W/(m·K)) and good oxidation resistance (up to 1400 °C) [2,5]. Furthermore, the thermal expansion coefficients of the two phases show only slight differences, i.e.  $8.1 \cdot 10^{-6} \text{ K}^{-1}$  and  $8.5 \cdot 10^{-6} \text{ K}^{-1}$  for  $\text{TiB}_2$  and  $\text{MoSi}_2$ , respectively [2,26].

Chromium silicide has been so far rarely used [5,27] as an additive to activate the sintering of boride ceramics. This compound is mainly characterised by its high oxidation resistance [5,27,29]. All these factors make both silicides potential activators of  $\text{TiB}_2$  sintering as well as additives which could favourably influence properties of boride ceramics.

## II. Experimental

$\text{TiB}_2$  powder from ABCR Company (GRADE F, cat. no. AB 134577) was used to make the samples.  $\text{CrSi}_2$  (ABCR Company, 99%, cat. no. AB 102105) and  $\text{MoSi}_2$  (Morton Thiokol, 99%, cat. no. 48108) powders were used as additives to activate  $\text{TiB}_2$  sintering. Particle size distribution of the powders was determined by the laser light diffraction method using Mastersizer 2000 (Malvern Instruments) and powder particle morphology was observed using Nova NanoSEM 200 scanning electron microscope (FEI Company).

The sintering experiments of  $\text{TiB}_2$  were performed using 10 wt.% addition of  $\text{CrSi}_2$  or  $\text{MoSi}_2$  which corresponds to 9.0 and 7.5 vol.%, respectively. Homogenization of the powder mixtures was carried out for 12 h in isopropyl alcohol, in a laboratory ball mill using spherical SiC grinding media. The resulting suspension was then placed under an IR irradiation to evaporate the alcohol. The dried mixture was subjected to

granulation using a nylon sieve. The powder mixtures were placed in a graphite die (diameter 2 inches; height 5 mm) and hot pressed (HP) in a Thermal Technology press. The HP sintering temperatures were 2050 °C for the  $\text{MoSi}_2$  containing sample and 1550 °C for  $\text{CrSi}_2$  containing sample, respectively. The sintering temperatures of various systems were selected on the basis of previous dilatometric investigations and the samples were sintered at 25 MPa under argon flow, the heating rate was 10 °C/min. The dwelling time at the maximum temperature was 1 h.

Apparent density of the sintered samples was measured using the Archimedes method. Specimens for microscopic observations were prepared by grinding and polishing (LaboForce-100, Struers Inc.).

A phase composition of the materials was determined by X-ray diffractometer Empyrean (PANalytical). The measurements were made using a monochromatic X-ray radiation with a wavelength corresponding to  $K_{\alpha 1}$  copper emission line (1.54178 Å) in the angular range 20–115° and 5–90° on the  $2\theta$  scale, a goniometer step of 0.008° with a scan rate of 0.003 °/s. A qualitative analysis of the phase composition was carried out using the X'Pert HighScore Plus computer programme, developed by PANalytical. Used databases were PDF-2 (2004) and ICSD Database FIZ Karlsruhe (2012). A quantitative phase composition of the materials was determined with the Rietveld method.

Observation of the samples' microstructure was carried out using Nova NanoSEM 200 scanning electron microscope (FEI Company). Microstructural analysis was performed with a scanning microscope using an ETD (Everhart-Thornley) detector.

The elemental composition of selected sample microareas was analysed using the EDS method. The Genesis XM X-ray microanalysis system (EDAX, Tilburg, the Netherlands) featuring the EDAX Sapphire Si(Li) EDS detector was used. Microstructure SEM observations were performed at an accelerating voltage of 18 kV but EDS analysis was carried out at 12 kV voltage. It should be noted that the EDS analysis was only qualitative.

The samples were characterized in terms of mechanical properties. The hardness of the materials was determined using the Vickers hardness method (FV-810, Future-Tech). Test load was 9.8 N and 10 indentations were made for each sample. Bending strength was measured with the three-point bending method using a universal testing machine (Z2.5, Zwick-Roell). Geometrical dimensions of the test samples for bending strength and fracture toughness were compliant with EN 846-1:2006 and EN ISO 15732:2005 standards, respectively.

The fracture toughness was determined using two methods, i.e. SENB notched beam three-point bending method (Z2.5, Zwick-Roell) and the Palmqvist cracking method with Vickers hardness tester (FV-810, Future-Tech). In case of the second method 10 indentations were made for each material using load of 29.5 N.

Young's modulus measurements were carried out with an ultrasonic method using UZP-1 testing apparatus (Inco-Veritas) equipped with a longitudinal waves transducer ( $f = 10$  MHz, with an oil as a coupling agent) or a transverse waves transducer ( $f = 2$  MHz, with a Canadian balsam as a coupling agent).

Oxidation resistance of the materials was determined by measuring the weight changes of samples heated in an air furnace at temperatures up to  $1400^\circ\text{C}$ . Cuboidal samples (beams) were placed on corundum substrates. The heating rate was  $5^\circ\text{C}/\text{min}$ , and samples were dwelled at  $1000$ ,  $1200$  and  $1400^\circ\text{C}$  for 2 h. Recorded weight changes ( $\Delta m$ ) of the samples were related to their surface area which was calculated from their geometrical dimensions. The oxidation susceptibility was presented as the  $\Delta m/A$  dependence (where  $A$  is an area of the oxidized sample) as a function of the oxidation temperature. The  $\text{TiB}_2$ - $\text{MoSi}_2$  sample which was oxidized at  $1400^\circ\text{C}$  disintegrated, thus in this case the maximum oxidation temperature was  $1200^\circ\text{C}$ . SEM observations and EDS chemical analysis as well as XRD analysis of the surface of samples oxidized at the maximum temperature were performed. Additionally, the SEM/EDS observations and analysis were performed on the polished oxidation cross-sections (profiles) of the samples.

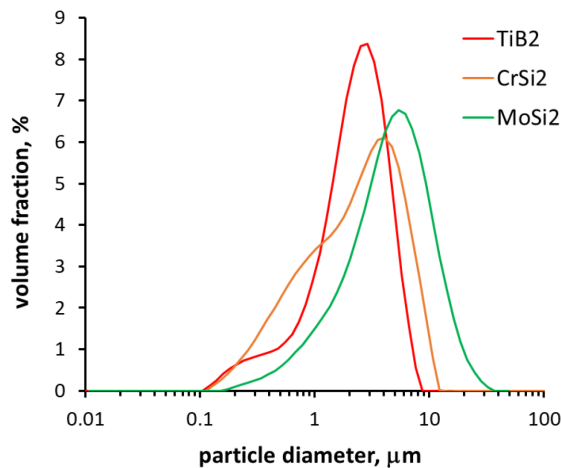


Figure 1. Particle size distribution of the  $\text{TiB}_2$ ,  $\text{CrSi}_2$  and  $\text{MoSi}_2$  powders

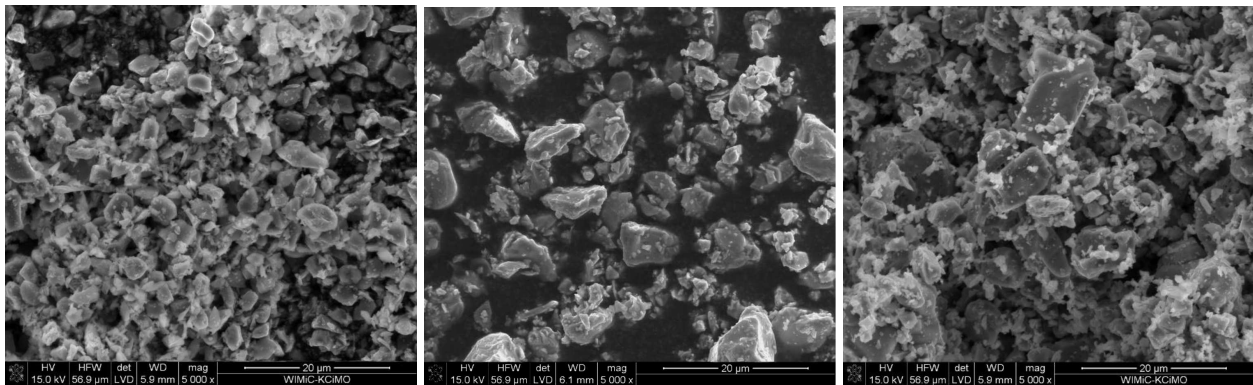


Figure 2. SEM micrographs showing morphology of: a)  $\text{TiB}_2$ , b)  $\text{MoSi}_2$  and c)  $\text{CrSi}_2$  powders

### III. Results and discussion

#### 3.1. Powders characteristics

The particle size distribution curve of the  $\text{TiB}_2$  powder (Fig. 1) shows that the dominant fraction represents particles in the range of  $2.5$ – $4.0\ \mu\text{m}$  and a small population of  $0.2$ – $0.3\ \mu\text{m}$  particles is also visible. The information obtained from the particle size distribution curve is confirmed by the SEM image of the powder morphology (Fig. 2a).

The particle size distributions of both silicide powders are also illustrated in Fig. 1, while their morphologies are shown in Figs. 2b and 2c. The dominant particle size of both silicide powders is similar (Figs. 1 and 2).

#### 3.2. Phase composition analysis

X-ray diffraction analysis of the sintered  $\text{TiB}_2$  sample with  $\text{MoSi}_2$  addition (Fig. 3) showed that the dominant phases are  $(\text{Mo,Ti})\text{B}_2$  solid solution and  $\text{TiB}_2$ . A small amount of silicon carbide (3C-SiC) was also identified, resulting from the reaction of molybdenum silicide with carbon [1,24,25,27], the presence of which is due to the graphite foil and the graphite die used for the hot pressing. However, no molybdenum silicide is identified after the sintering.

Analysis of phase composition of the sintered  $\text{TiB}_2$  sample with  $\text{CrSi}_2$  (Fig. 4) showed that  $\text{TiB}_2$  dominates in the resulting composite. Insignificant amounts

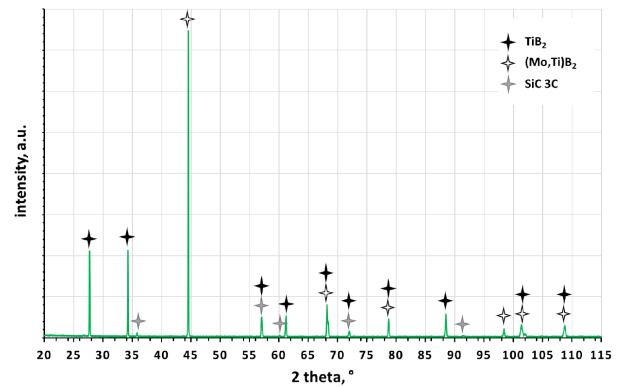


Figure 3. Diffraction pattern of  $\text{TiB}_2$  sample with the addition of  $\text{MoSi}_2$  ( $T = 2050^\circ\text{C}$ )

**Table 1. Theoretical ( $\rho_{th}$ ) and apparent ( $\rho_{ap}$ ) densities and open porosity of the hot-pressed ceramics**

Initial composition	$\rho_{th}^{\#}$ [g/cm <sup>3</sup> ]	$\rho_{ap}$ [g/cm <sup>3</sup> ]	Water absorption [%]	Phase composition [wt.%]	$\rho_{th}^*$ [g/cm <sup>3</sup> ]
TiB <sub>2</sub> -10 wt.% MoSi <sub>2</sub> (TiB <sub>2</sub> -7.5 vol.% MoSi <sub>2</sub> )	4.65	4.40 ± 0.02	0.05 ± 0.01	TiB <sub>2</sub> 74.0 (Mo,Ti)B <sub>2</sub> 23.2 SiC 2.8	4.73
TiB <sub>2</sub> -10 wt.% CrSi <sub>2</sub> (TiB <sub>2</sub> -9 vol.% CrSi <sub>2</sub> )	4.55	4.21 ± 0.06	0.08 ± 0.02	TiB <sub>2</sub> 78.5 (Cr,Ti)B <sub>2</sub> 11.6 CrSi <sub>2</sub> 5.2, SiO <sub>2</sub> 4.7	4.35

# theoretical density calculated from the rule of mixtures where TiB<sub>2</sub> = 4.52 g/cm<sup>3</sup>, CrSi<sub>2</sub> = 4.99 g/cm<sup>3</sup>, MoSi<sub>2</sub> = 6.3 g/cm<sup>3</sup>, (Mo,Ti)B<sub>2</sub> = 6.05 g/cm<sup>3</sup>, (Cr,Ti)B<sub>2</sub> = 4.75 g/cm<sup>3</sup>

\* theoretical density calculated from the phase composition

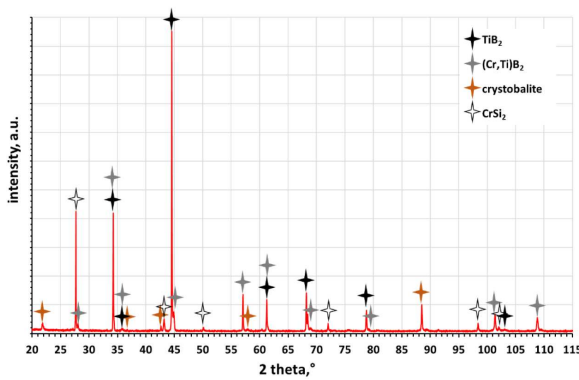


**Figure 4. A diffraction pattern of a TiB<sub>2</sub> sample with the addition of CrSi<sub>2</sub> ( $T = 1550\text{ }^{\circ}\text{C}$ )**

of phases such as (Cr,Ti)B<sub>2</sub> solid solution and the high-temperature polymorphic SiO<sub>2</sub> cristobalite, were also formed [27]. A residual additive CrSi<sub>2</sub> is also identified in the sintered sample.

Apparent density and water absorption of the hot-pressed samples are shown in Table 1. The table shows also theoretical density of the composites both calculated from their initial composition and calculated from the phase composition of the sintered samples.

### 3.3. Density measurements

The TiB<sub>2</sub> sample with MoSi<sub>2</sub> additive shows a slightly higher apparent density. Reliable calculation of relative density of the composite materials poses many difficulties. During the sintering, numerous reactions take place between titanium diboride, the silicides and oxide impurities as evidenced by the phase composition analyses (Figs. 3 and 4; Table 1). Therefore, taking the density calculated from the initial compositions as the theoretical density of a given material seems to be incorrect. On the other hand, calculation of the theoretical density from the phase composition analyses, due to the presence of solid solutions, is also subjected to sig-

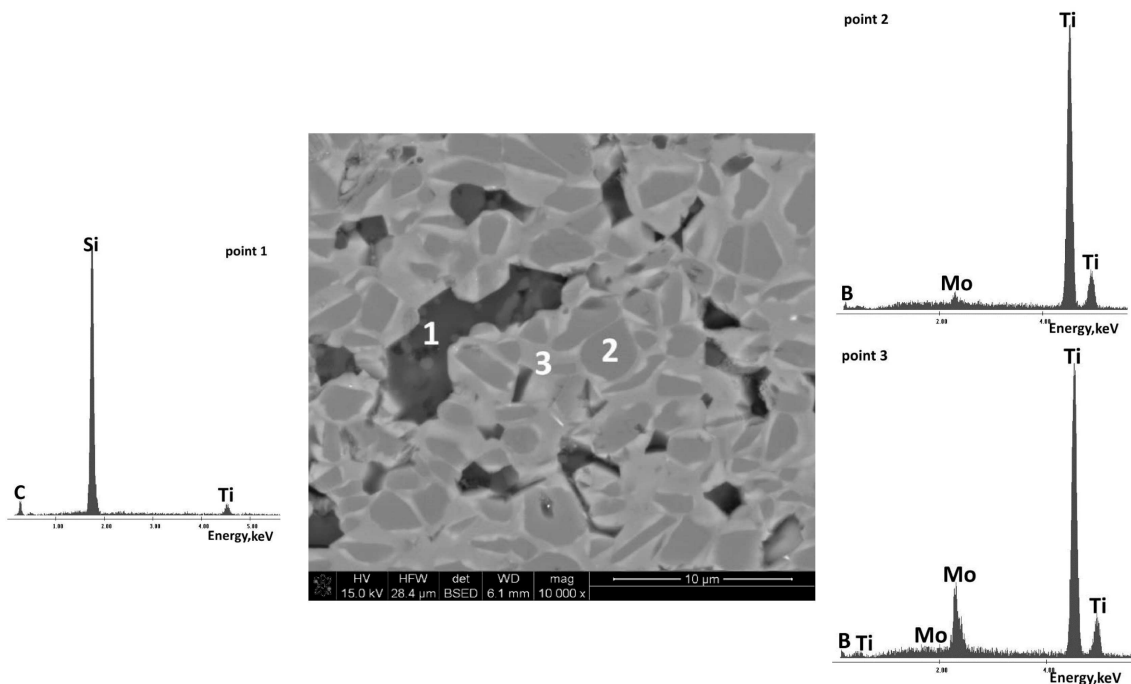


**Figure 5. SEM image of the MoSi<sub>2</sub>-TiB<sub>2</sub> sample with the locations where EDS chemical composition analyses were performed and the corresponding results of EDS analysis**

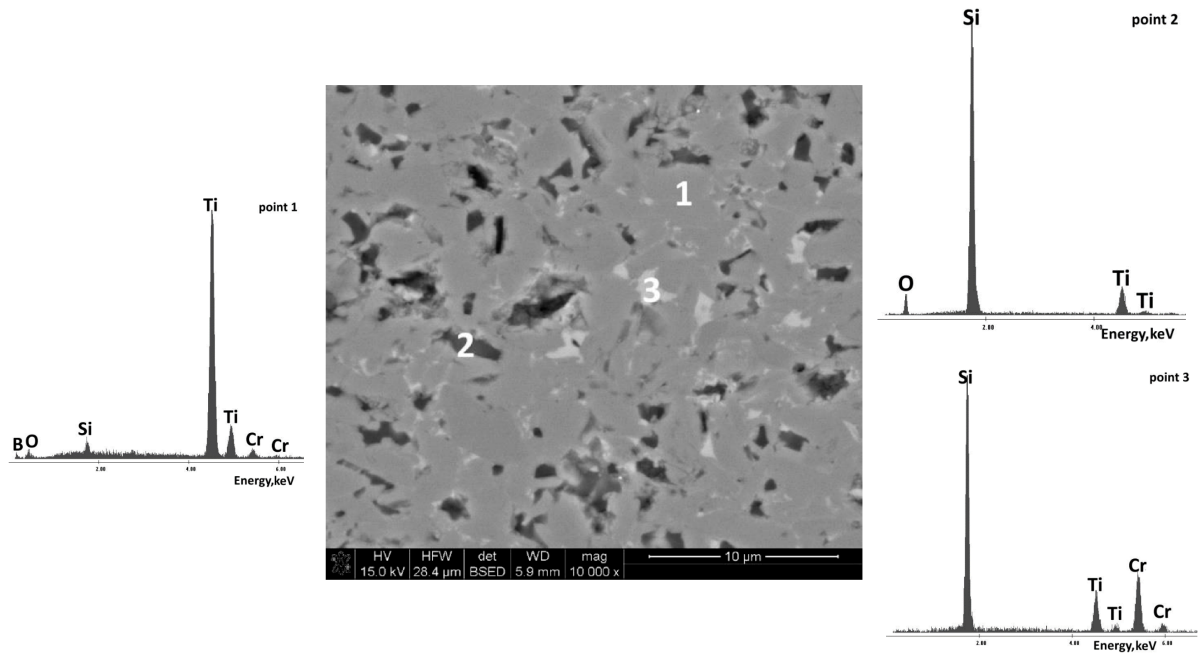


Figure 6. SEM image of the CrSi<sub>2</sub>-TiB<sub>2</sub> sample with the locations where EDS chemical composition analyses were performed and the corresponding results of EDS analysis

nificant error. Thus, on the basis of the apparent density and water absorption measurements, it can be concluded that the materials have negligible open porosity, as evidenced by the low water absorption of both composites (Table 1).

### 3.4. Microstructure and chemical composition

SEM micrographs of the sintered samples are shown in Figs. 5 and 6. The microstructure of the polycrystalline TiB<sub>2</sub> with MoSi<sub>2</sub> (Fig. 5) resembles the structure of cermets, i.e. materials with the general formula (Ti,Me)(C,N) with Co or Ni additives, where Me = Mo, W, Ta, Nb, V, Al. In the cermets, particles of the hard phase are embedded in the plastic (metallic) binder, resulting in a characteristic core-shell structure. A shell sometimes has several layers, differing in chemical composition [27,30]. In a case of the observed sample, layers around the core that significantly differ in a shade of grey can be seen, suggesting their different chemical composition. When analysing the SEM images of the TiB<sub>2</sub> sample with CrSi<sub>2</sub> (Fig. 6), areas differing in grey scale can also be observed. In the case of both polycrystals, it can be concluded that the darkest areas are pores or grains torn out during the mechanical processing, i.e. grinding.

The results of EDS analysis of the three micro areas of the composite with MoSi<sub>2</sub> additive are shown in Fig. 5. The micro-area marked by point 1 is rich in silicon and carbon as well as titanium (Fig. 5). This phase is probably silicon carbide which is formed by reactions between molybdenum silicide and carbon from the reactor, the graphite die and graphite lining foil. EDS analysis showed that the core of the resulting composite (Fig. 5; point 2) is TiB<sub>2</sub>. The shell (Fig. 5) is a phase rich in titanium, molybdenum and boron, probably the (Mo,Ti)B<sub>2</sub> solid solution identified by the XRD analysis.

The results of EDS analysis of the three micro areas of the TiB<sub>2</sub>-CrSi<sub>2</sub> composite are shown in Fig. 6. Based on the chemical composition analysis, the area marked with point 1 (Fig. 6) is most likely titanium diboride. The area marked by point 2 (Fig. 6) on the other hand, is rich in silicon as well as smaller amounts of titanium and oxygen. The micro-area marked with point 3 (Fig. 6) is rich in silicon, titanium and chromium and may be the residue of the additive chromium silicide. Also in the case of the TiB<sub>2</sub>-CrSi<sub>2</sub> system, reactions can occur during sintering, leading to the formation of various phases visible in the microstructure of the sintered body and identified by phase composition analysis.

Table 2. Results of flexural strength ( $\sigma$ ), Vickers hardness ( $H_v$ ), Young's modulus ( $E$ ) and fracture toughness tests

Sample	$\sigma$ [MPa]	$H_v$ [GPa]	$E$ [GPa]	Average $K_{Ic}$ value [MPa·m <sup>0.5</sup> ]	
				indentation method	SENB method
TiB <sub>2</sub> single-phase*	300–450	20–30	400–500	4.0–6.0	
TiB <sub>2</sub> -MoSi <sub>2</sub>	487 ± 24.5	21.9 ± 2.8	459.9 ± 7.6	5.9 ± 0.4	4.7 ± 0.3
TiB <sub>2</sub> -CrSi <sub>2</sub>	432 ± 22.0	20.5 ± 1.8	447.0 ± 10.6	5.4 ± 0.2	5.4 ± 0.3

\* the literature data [1,3,5,24,27,31,32,33]

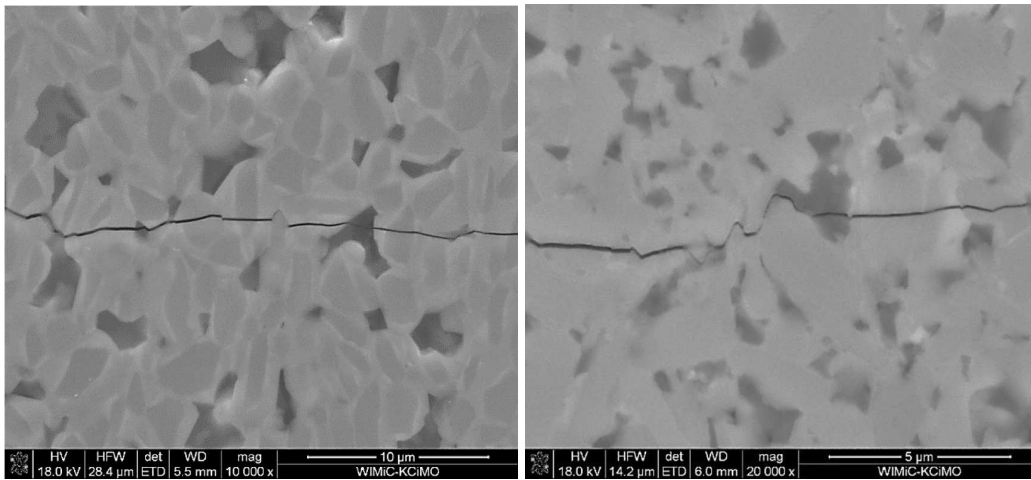


Figure 7. SEM images of fracture path in composites: a)  $\text{TiB}_2\text{-MoSi}_2$  and b)  $\text{TiB}_2\text{-CrSi}_2$

### 3.5. Mechanical properties

Table 2 summarizes the mechanical properties and presents the results of: bending strength, Vickers hardness, fracture toughness and Young modulus measurements. The fracture toughness was measured by using two measurement methods, i.e. the three-point notched beam bending method (SENB) and the indentation method. For both tested composites as well as for both methods used, similar fracture toughness results were obtained, which oscillate around  $5 \text{ MPa}\cdot\text{m}^{0.5}$ . In Fig. 7, the crack path in both composites was illustrated using SEM. It can be observed that the fracture runs both through the grains and is also deflected by the hard cores of the boride phase (Fig. 7).

### 3.6. Oxidation resistance

In the temperature range 1000–1200 °C, an increase in mass can be observed for both samples (Fig. 8).

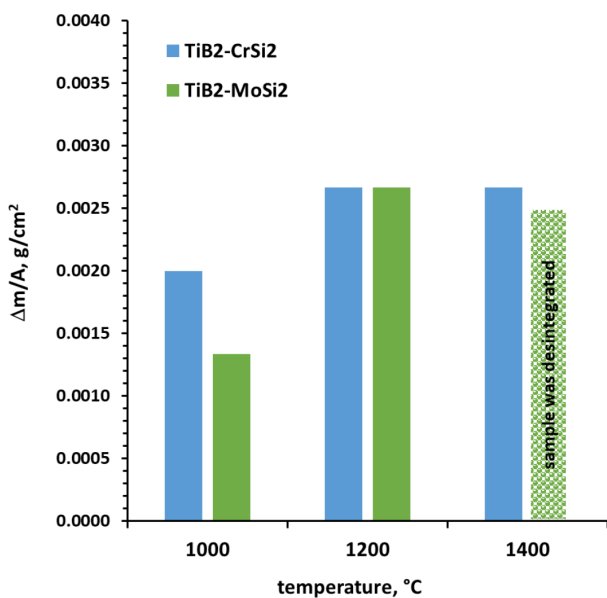


Figure 8. Mass changes related to the surface area of the oxidized  $\text{TiB}_2$  samples with  $\text{MoSi}_2$  and  $\text{CrSi}_2$  additives

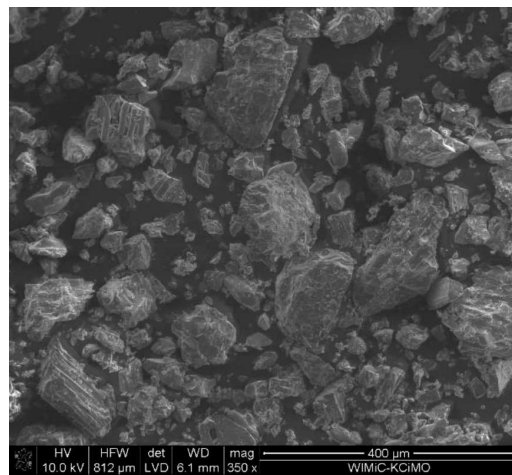


Figure 9. Remains of the  $\text{TiB}_2\text{-MoSi}_2$  sample oxidized at 1400 °C

The weight increase reaches slightly more than  $2.5 \cdot 10^{-3} \text{ g/cm}^2$ , once the temperature exceeds 1200 °C. Further heating of the samples in the case of the sample with  $\text{CrSi}_2$  does not increase the weight gain of the sample, while the sample with  $\text{MoSi}_2$  disintegrates (Fig. 9).

Figure 10 shows XRD diffraction patterns of the oxidized samples. SEM micrographs of the oxidized cross section, together with chemical composition analyses, are illustrated in Fig. 11 which shows the oxidation cross-section of the  $\text{TiB}_2\text{-MoSi}_2$  composite oxidized at 1200 °C. The oxidation cross-section of  $\text{TiB}_2\text{-CrSi}_2$  composite oxidized at 1400 °C is shown in Fig. 12. Based on the SEM observations and the XRD and EDS analyses, stable oxides mainly  $\text{TiO}_2$  and  $\text{SiO}_2$  and  $\text{SiO}_2$ -rich amorphous phases can be identified on the oxidized surface of both materials (Figs. 10 and 11). Beneath the amorphous-crystalline layers, a sublayer composed mainly of  $\text{SiO}_2$  can be observed, with substitutions or very fine Mo or Cr particles (Figs. 10a and 11).

A surface of the  $\text{TiB}_2\text{-CrSi}_2$  sample (Fig. 12) was tightly covered by a layer of a oxidation product. In both materials up to 1200 °C the oxidation had a passive nature. Regarding the sample with  $\text{MoSi}_2$ , it is reasonable

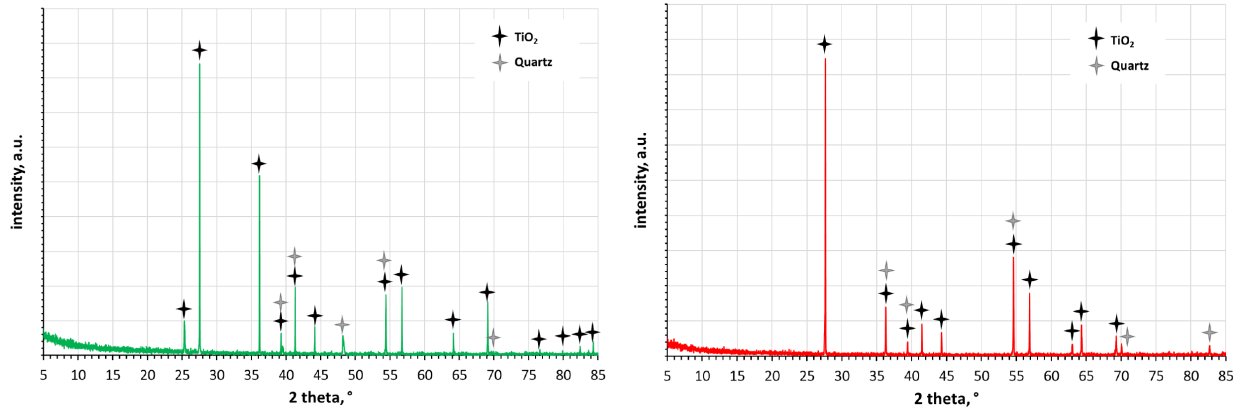


Figure 10. XRD analysis of the oxidized sample surfaces: a)  $\text{TiB}_2\text{-MoSi}_2$  at  $1200\text{ }^\circ\text{C}$  and b)  $\text{TiB}_2\text{-CrSi}_2$  at  $1400\text{ }^\circ\text{C}$

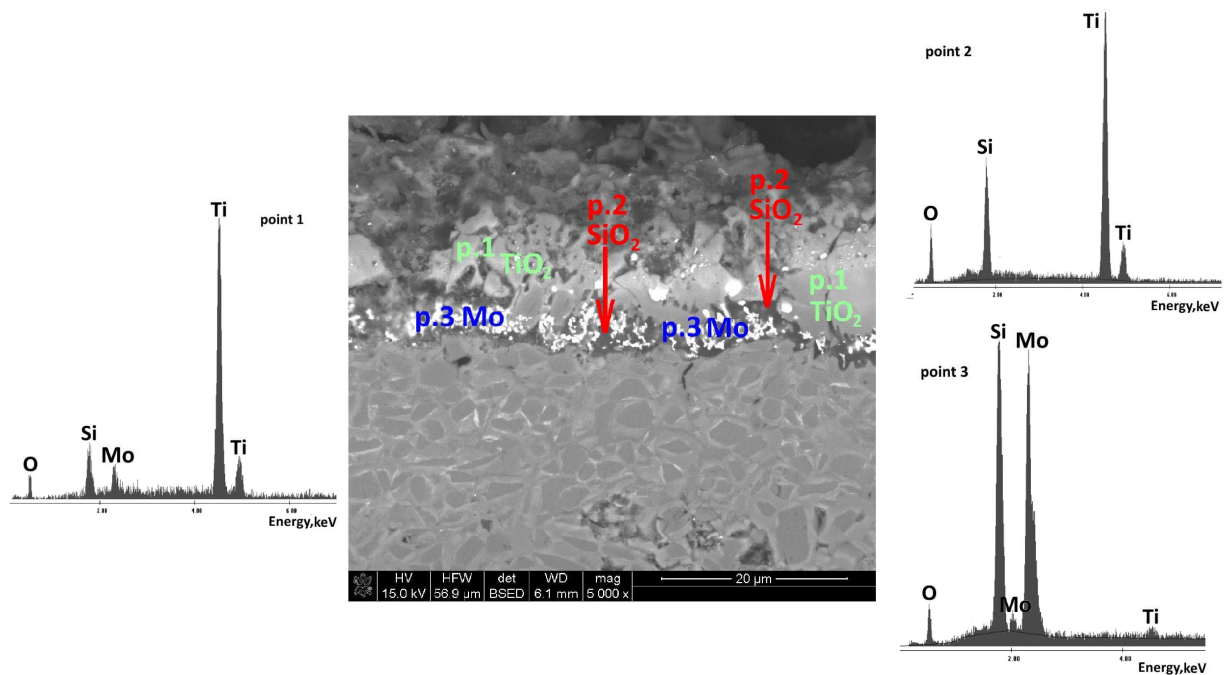


Figure 11. SEM microphotographs of a sample cross-section after the oxidation at  $1200\text{ }^\circ\text{C}$  and chemical composition analysis of the micro-areas of the oxidation residues for the sample  $\text{TiB}_2\text{-MoSi}_2$

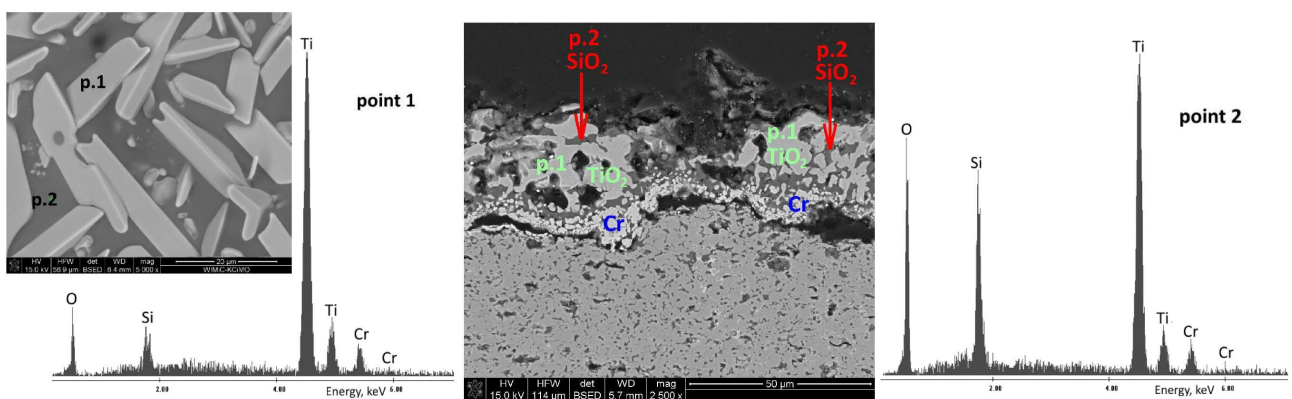


Figure 12. SEM microphotographs of the surface oxidized at  $1400\text{ }^\circ\text{C}$  and chemical composition analysis of the micro-areas for the sample  $\text{TiB}_2\text{-CrSi}_2$  as well as the oxidation cross-section

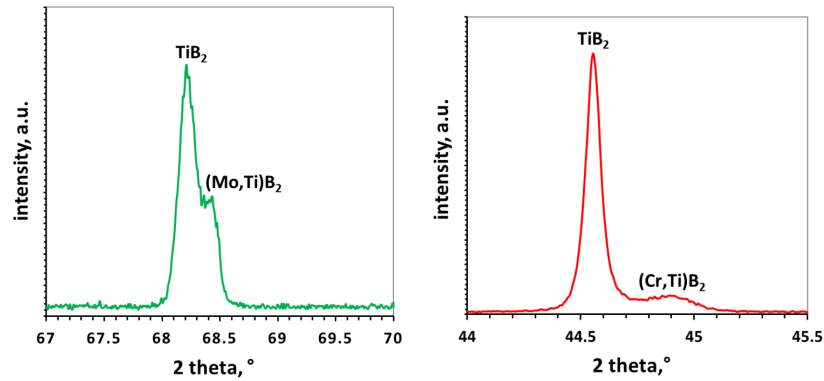


Figure 13. A section of the X-ray pattern proving the existence of solid solutions: a) (Mo,Ti)B<sub>2</sub> and b) (Cr,Ti)B<sub>2</sub>

Table 3. Parameters of unit cell of TiB<sub>2</sub> and (Mo,Ti)B<sub>2</sub> as well as (Cr,Ti)B<sub>2</sub> determined from the XRD measurements

	Theoretical cell parameters of TiB <sub>2</sub> according to Ref. 35 [Å]	Cell parameters for sample TiB <sub>2</sub> with MoSi <sub>2</sub> [Å]	Cell parameters for sample TiB <sub>2</sub> with CrSi <sub>2</sub> [Å]
TiB <sub>2</sub> phase	$a = 3.028$ $b = 3.028$ $c = 3.228$	$a = 3.029$ $b = 3.029$ $c = 3.231$	$a = 3.028$ $b = 3.028$ $c = 3.230$
(X,Ti)B <sub>2</sub> phase (where X = Mo or Cr)		$a = 3.033$ $b = 3.033$ $c = 3.225$	$a = 3.021$ $b = 3.021$ $c = 3.188$

to assume that above 1200 °C there is a change from a passive to an active oxidation. As a result of the formation of significant quantities of gaseous products of MoSi<sub>2</sub> decomposition (formation of volatile MoO<sub>3</sub>), the continuity of the tight oxide layer formed on the surface is discontinued, leading to a change in the nature of oxidation from passive to active. This phenomenon is not observed in the case of the samples with CrSi<sub>2</sub> additive.

#### IV. Discussions

The study shows (XRD, SEM+EDS) that the formed polycrystals are multiphase systems (Figs. 3–6). During the sintering process, different phases are formed which are difficult to identify unambiguously and even more so to determine their quantity, and thus to determine the weighted (real) density necessary to calculate the total. Therefore, it can be assumed that the apparent density of the sintered bodies is higher than the calculated one. Analysis of SEM microphotographs (Figs. 5 and 6) confirms this conjecture, since the darkest areas, visible in the images as shown by the EDS analysis, are not only pores.

Analysis of the phase composition (Figs. 3 and 4) confirms that titanium boride is the dominant phase for both sintered samples. The introduced silicide additives, if they remain in the sinter, are in small amounts and mostly react with the boride and oxide impurities. Solid solutions of (Mo or Cr,Ti)B<sub>2</sub>, silicide residues, silicon carbide as well as cristobalite (SiO<sub>2</sub>) can be identified in the sintered material (Figs. 3 and 4).

Formation of solid solutions is evidenced by broad-

ening and shape of peaks (Fig. 13) as well as significant changes in parameters of the TiB<sub>2</sub> unit cell (Table 3). An example of a distorted or doubled peaks indicating the formation of (Mo,Ti)B<sub>2</sub> or (Cr,Ti)B<sub>2</sub> solid solutions is shown in Fig. 13. Also, the changes in the parameters of the TiB<sub>2</sub> unit cell, presented in Table 3, confirm the possibility of formation of (Mo,Ti)B<sub>2</sub> and (Cr,Ti)B<sub>2</sub> solid solutions. A significant increase of lattice parameters is observed, which is probably related to the incorporation of Mo cations into the TiB<sub>2</sub> structure. In contrast, a reduction in the unit cell size is observed for the (Cr,Ti)B<sub>2</sub> solid solution due to smaller atomic radius size of chromium [34] (Table 3).

TiB<sub>2</sub>, MoSi<sub>2</sub>, CrSi<sub>2</sub> as well as impurities predominantly in the form of oxide TiO<sub>2</sub> and B<sub>2</sub>O<sub>3</sub> are present in the initial systems. During sintering, several chemical reactions are possible between TiB<sub>2</sub>, silicides and the oxide impurities, e.g. TiO<sub>2</sub> and B<sub>2</sub>O<sub>3</sub>. The reactions can result in the formation of titanium silicides, monoborides as well as complex metal, silicon and boron compounds [1,5,29,31,36–38]. In addition, as reported in the literature [1,36,37], partial dissolution of Mo or Cr in TiB<sub>2</sub> is possible in the temperature range 1350–1930 °C. A liquid phase (Mo,Cr)-Ti-B-O is formed, from which a solid solution (Me,Ti)B<sub>2</sub> (where Me = Mo or Cr) precipitates during cooling at the grain boundaries or, more commonly, at the surface of the boride particles. Such epitaxial precipitation can be observed (Fig. 5) in the case of polycrystalline TiB<sub>2</sub> with MoSi<sub>2</sub> additive. The microstructure of this composite is similar to cermets, with a core and a rim visible in the particles (Fig. 5). According to the literature [1,5,29,36,38],

the presence of liquid phases during sintering is evidenced by the occurrence of solid solutions in the sintered material, as well as boride, silicide, and silicide-boride phases. In addition, the formation of titanium silicide is possible, which, according to literature data [1,4], undergoes melting at around 1500 °C.

Titanium silicide and other silicides and borides were not found in the sintered composites. In contrast, according to the available data, chromium silicide melts between 1450 and 1490 °C, and molybdenum silicide at 2030 °C [1,5,29]. It can therefore be postulated that, irrespective of the type of silicide additive used, it is possible for liquid phases to appear and to activate TiB<sub>2</sub> sintering [1,36,37]. This is evidenced by the phases present in the composites after sintering identified by the XRD analysis (Figs. 3 and 4) and the EDS micro-area chemical composition analysis (Figs. 5 and 6).

In addition, it should be noted that during sintering, interactions of all components with the surrounding carbon-rich environment, i.e. with the graphite lining, heating elements and a graphite die, are possible. Evidence for this is the silicon carbide identified in the sample sintered with MoSi<sub>2</sub> addition (Figs. 3 and 5).

As a result of the reactions between the starting components, the formation of SiO<sub>2</sub> is possible. Small amounts of the high-temperature SiO<sub>2</sub> variety, i.e. cristobalite were identified in the sample sintered with addition of CrSi<sub>2</sub> (Fig. 4). In this case, the formation of SiO<sub>2</sub> is favoured at the sintering temperature of 1550 °C, which is low for the sintering of boride ceramics.

The density measurements do not provide knowledge about the actual porosity of the composites. Observations of the microstructure also give a misleading picture; the sintered bodies are most likely less porous as the pictures show. Because the microstructure image is complex, it is difficult to obtain the correct phase contrast despite the use of different SEM detectors. The number, size and shape of the pores which are the stress-concentrating defects mainly determine the mechanical parameters measured in the work. The determined values of flexural strength, Young's modulus, hardness and fracture toughness are comparable to those reported in the literature as well as to the ones recorded for single-phase TiB<sub>2</sub> polycrystals [1,3,5,24,27,31,32]. Both composites have similar hardness of about 21 GPa and bending strength oscillating around 450 MPa. The Young's modulus is about 450 GPa which indicates low deformability of the composites (Table 2). Noteworthy is the high fracture toughness of both composites, which, expressed by the critical stress intensity factor, is in the range of 4.5–5.5 MPa·m<sup>0.5</sup>. Figure 8 illustrates the crack propagations and it is possible to observe phenomena that significantly increase the effective fracture energy. It can be observed that the crack propagation through the grains of the hard but brittle boride phase occurs. The phenomenon leading to the increase in effective fracture energy is mainly the deflection of the crack propagation at the grain boundaries (Fig. 8) and within

the phases formed by the reaction of TiB<sub>2</sub> with the additives and impurities (Fig. 8).

In the available literature [1–3,5,24–26] there are many papers describing TiB<sub>2</sub>-MoSi<sub>2</sub> composites, while the number of papers discussing TiB<sub>2</sub>-CrSi<sub>2</sub> composites remains small [27] despite the promising oxidation resistance results of the latter composites. Up to now, the maximum operating temperature at which the oxidation resistance of TiB<sub>2</sub>-CrSi<sub>2</sub> composites was tested was 950 °C. One of the main objectives of the present work was to compare the oxidation resistance of the most common, silicide-based TiB<sub>2</sub>-MoSi<sub>2</sub> composite with the promising TiB<sub>2</sub>-CrSi<sub>2</sub> composite at much higher operating temperatures. According to the literature data [5,36,38,39], the reaction of oxygen with TiB<sub>2</sub> and MoSi<sub>2</sub> during oxidation can result in the formation of titanium silicide, boron oxide B<sub>2</sub>O<sub>3</sub> and molybdenum oxide MoO<sub>3</sub>. At temperatures up to 1000 °C, the formation of protective amorphous layers of B<sub>2</sub>O<sub>3</sub>-TiO<sub>2</sub> and B<sub>2</sub>O<sub>3</sub>-SiO<sub>2</sub> is possible; in the case of a sample with CrSi<sub>2</sub>, the protective layers can be enriched with Cr<sub>2</sub>O<sub>3</sub>. Heating the samples at temperatures higher than 1000 °C leads to the transition of B<sub>2</sub>O<sub>3</sub> and MoO<sub>3</sub> oxides into the gas phase. Both oxides show high partial pressures where boron oxide between 1000 and 1200 °C transits into the gas phase, and molybdenum oxide already at 500 °C shows high partial pressure [3,36,38]. In the phase composition of the oxidized surfaces of both composites (Fig. 10), refractory oxides such as TiO<sub>2</sub> and SiO<sub>2</sub> can be identified. In the case of the TiB<sub>2</sub>-CrSi<sub>2</sub> sample, the XRD pattern shows that TiO<sub>2</sub> crystals and quartz crystals are formed on the surface (Fig. 10b). Further oxidation of the TiB<sub>2</sub>-MoSi<sub>2</sub> sample above 1200 °C leads to the destruction of the passivation protective layer and formation of molybdenum oxides (primarily MoO<sub>3</sub>), which exhibit high volatility. In this case, it can be concluded that above 1200 °C oxidation changes from a passive to an active character (Fig. 8), leading to the decomposition of the TiB<sub>2</sub>-MoSi<sub>2</sub> sample (Fig. 9).

Figure 11 shows the oxidation cross-section of the TiB<sub>2</sub>-MoSi<sub>2</sub> sample at 1200 °C, together with an analysis of the chemical composition of the micro-areas in the layer. A porous passivation layer probably composed of a SiO<sub>2</sub>-rich amorphous phase with present TiO<sub>2</sub> grains and dissolved molybdenum is visible on the surface (Fig. 11). Going deeper into the sample, only TiO<sub>2</sub>-SiO<sub>2</sub> oxides are present in the layer (Fig. 11). Molybdenum is again present in the SiO<sub>2</sub>-rich sublayer between the interior of the sample and the oxide layer (Fig. 11). The absence of molybdenum oxide in the oxidation cross-section indirectly demonstrates the high volatility of MoO<sub>3</sub>. The analyses further indicate that the layer visible in Fig. 11 does not protect the sample from further oxidation.

In the case of CrSi<sub>2</sub> addition, the high oxidation resistance is retained. The layer formed on the sample surface tightly covers the sample surface preventing further oxidation of the sample. According to the XRD analysis

(Fig. 10b), oxides of  $\text{TiO}_2$  and  $\text{SiO}_2$  (quartz) are identified on the sample surface. The background increase observed in the XRD also indicates the presence of an amorphous phase originating most likely from the  $\text{SiO}_2$  (Fig. 12). It is conceivable that an amorphous borosilicate glass layer is formed as a result of the reaction between the resulting  $\text{SiO}_2$  and  $\text{B}_2\text{O}_3$  oxides, providing better surface protection to the composite due to the lower volatility of this phase in relation to the original oxides forming it. Also it forms a tighter layer protecting the surface of the composite by slowing down the diffusion of oxygen into the surface of the material [40–43]. Observations of the oxidized surface (Fig. 12) show the presence of crystals embedded in a tightly covered layer, probably amorphous (Fig. 12), on the surface of the sample. Based on EDS chemical analysis, these crystals are titanium oxide (Fig. 12), identified by the XRD analysis (Fig. 10b). The oxidation cross-section shown in Fig. 12 confirms that the surface of the sample is covered by an amorphous  $\text{SiO}_2$  (dark grey areas), in which  $\text{TiO}_2$  crystals are present (light grey areas) (Fig. 12). In the case of  $\text{TiB}_2$ - $\text{CrSi}_2$  composites, a chromium-rich and  $\text{SiO}_2$ -rich sublayer is present between the tight outer layer and the interior of the sample (Fig. 12).

These observations are consistent with the literature data on the oxidation resistance of  $\text{TiB}_2$  composites with additions of various silicides. According to these data, the additive that significantly increases the oxidation resistance is  $\text{CrSi}_2$ , while the addition of  $\text{MoSi}_2$  has an unfavourable effect due to the destruction of the passivation layer as a result of  $\text{MoO}_3$  evaporation [3,36,38]. The oxidation scheme of the two composites is illustrated in Fig. 14.

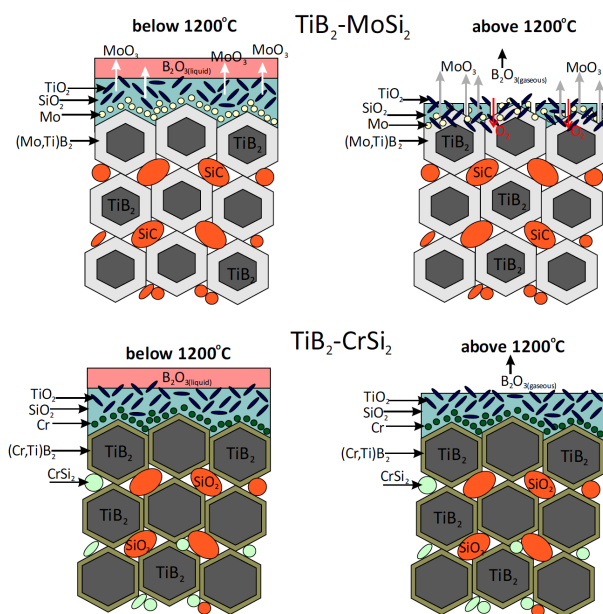


Figure 14. Oxidation scheme of both composites

## V. Conclusions

The paper presents a successful attempt to obtain dense  $\text{TiB}_2$ -based ceramics. Molybdenum and chromium silicides were used as sintering-activating additives. According to the literature data, it was found that a variety of densification-activating liquid phases is formed during sintering due to the introduced additives. As a result of the reaction between  $\text{TiB}_2$  and  $\text{MeSi}_2$  ( $\text{Me} = \text{Cr}, \text{Mo}$ ), solid solutions of  $(\text{Me}, \text{Ti})\text{B}_2$  are formed, resulting in interesting cermet-type microstructures. The mechanical properties of the resulting multiphase materials do not differ from those of single-phase  $\text{TiB}_2$ , and some of them, such as fracture toughness and oxidation resistance, can even be considered superior. A promising additive appears in the seldom use of chromium silicide  $\text{CrSi}_2$ . With this additive, dense ceramics with good mechanical and chemical properties are obtained at  $1550^\circ\text{C}$  which is a low temperature for the  $\text{TiB}_2$ -type ceramics with a dominant strong covalent bond.

**Acknowledgements:** The work was carried out under the project Excellence Initiative - Research University (AGH-University of Science and Technology, Krakow, Poland) of number: 501.D4.II.696.7996 and subsidy from the Ministry of Education and Science to the AGH University of Science and Technology in Krakow (project no 16.16.160.557).

## References

1. T.S.R.C. Murthy, B. Basu, R. Balasubramaniam, A.K. Suri, C. Subramanian, R.K. Fotedar, "Processing and properties of  $\text{TiB}_2$  with  $\text{MoSi}_2$  sinter-additive: A first report", *J. Am. Ceram. Soc.*, **89** (2006) 131–138.
2. R. Riedel, *Handbook of Ceramic Hard Materials*, Wiley-VCH, Weinheim, New York, 2000.
3. B.R. Golla, A. Mukhopadhyay, B. Basu, S.K. Thimmappa, "Review on ultra-high temperature boride ceramics", *Prog. Mater. Sci.*, **111** (2020) 100651.
4. G.B. Raju, B. Basu, "Densification, sintering reactions, and properties of titanium diboride with titanium disilicide as a sintering aid", *J. Am. Ceram. Soc.*, **90** (2007) 3415–3423.
5. A. Suri, N. Krishnamurthy, C. Subramanian, "Issues in the synthesis and fabrication of refractory carbides, borides, silicides and their mixtures", pp. 69–79 in *Adv. Process. Manuf. Technol. Struct. Multifunct. Mater. II*, Eds. T. Ohji, M. Singh. John Wiley & Sons, Inc, Hoboken, New Jersey, 2010.
6. M.K. Ferber, P.F. Becher, C.B. Finch, "Effect of microstructure on the properties of  $\text{TiB}_2$  ceramics", *J. Am. Ceram. Soc.*, **66** (1983) C2–C3.
7. S.H. Kang, D.J. Kim, E.S. Kang, S.S. Baek, "Pressureless sintering and properties of titanium diboride ceramics containing chromium and iron", *J. Am. Ceram. Soc.*, **84** (2001) 893–895.
8. E.S. Kang, C.W. Jang, C.H. Lee, C.H. Kim, D.K. Kim, "Effect of iron and boron carbide on the densification and mechanical properties of titanium diboride ceramics", *J. Am. Ceram. Soc.*, **72** (1989) 1868–1872.
9. L.-H. Li, H.-E. Kim, E. Son Kang, "Sintering and

- mechanical properties of titanium diboride with aluminum nitride as a sintering aid”, *J. Eur. Ceram. Soc.*, **22** (2002) 973–977.
10. R. Telle, S. Meyer, G. Petzow, E.D. Franz, “Sintering behaviour and phase reactions of  $TiB_2$  with  $ZrO_2$  additives”, *Mater. Sci. Eng. A*, **105-106** (1988) 125–129.
  11. Y. Muraoka, M. Yoshinaka, K. Hirota, O. Yamaguchi, “Hot isostatic pressing of  $TiB_2$ - $ZrO_2$  (2 mol%  $Y_2O_3$ ) composite powders”, *Mater. Res. Bull.*, **31** (1996) 787–792.
  12. S. Torizuka, T. Kishi, “Effect of SiC and  $ZrO_2$  on sinterability and mechanical properties of titanium nitride, titanium carbonitride and titanium diboride”, *Mater. Trans. JIM*, **37** (1996) 782–787.
  13. T. Graziani, A. Bellosi, “Sintering and characterization of  $TiB_2$ - $B_4C$ - $ZrO_2$  composites”, *Mater. Manuf. Process.*, **9** (1994) 767–780.
  14. S. Torizuka, J. Habada, H. Nishio, “High strength  $TiB_2$ ”, pp. 1454–1460 in: *14<sup>th</sup> Annual Conference on Composites and Advanced Ceramic Materials: Ceramic Engineering and Science Proceedings*. Ed. J.B. Wachtman. John Wiley & Sons, Inc, Hoboken, NJ, USA, 1990.
  15. J. Schneider, K.H. Zum Gahr, R. Müller, E. Franz, “Einfluß des  $ZrO_2$ -Zusatzes auf mechanische Eigenschaften und den ungeschmierten Gleitverschleiß von  $TiB_2$ - $ZrO_2$ -Mischkeramiken”, *Materwissenschaft und Werkstofftechnik*, **27** (1996) 359–366.
  16. S. Torizuka, K. Sato, J. Harada, H. Yamamoto, H. Nishio, “Microstructure and sintering mechanism of  $TiB_2$ - $ZrO_2$ -SiC composite”, *J. Ceram. Soc. Jpn.*, **100** (1992) 392–397.
  17. S. Torizuka, K. Sato, H. Nishio, T. Kishi, “Effect of SiC on interfacial reaction and sintering mechanism of  $TiB_2$ ”, *J. Am. Ceram. Soc.*, **78** (1995) 1606–1610.
  18. D.F. Rodríguez-Rojas, V. Zamora, F. Guiberteau, A.L. Ortiz, “Solid-state spark plasma sintering of super wear resistant  $B_4C$ -SiC- $TiB_2$  triplex-particulate composites”, *Ceram. Int.*, **49** (2023) 5532–5537.
  19. J.-H. Park, Y.-H. Koh, H.-E. Kim, C.S. Hwang, E.S. Kang, “Densification and mechanical properties of titanium diboride with silicon nitride as a sintering aid”, *J. Am. Ceram. Soc.*, **82** (2004) 3037–3042.
  20. C.E. Holcombe, N.L. Dykes, “Microwave sintering of titanium diboride”, *J. Mater. Sci.*, **26** (1991) 3730–3738.
  21. E.S. Kang, C.H. Kim, “Improvements in mechanical properties of  $TiB_2$  by the dispersion of  $B_4C$  particles”, *J. Mater. Sci.*, **4** (1989) 580.
  22. Y. Murata, H.P. Julien, E.D. Whitney, “Densification and wear resistance of ceramic systems: I. Titanium diboride”, *Ceram. Bull.*, **46** (1967) 643–648.
  23. S.K. Bhaumik, C. Divakar, A.K. Singh, G.S. Upadhyaya, “Synthesis and sintering of  $TiB_2$  and  $TiB_2$ -TiC composite under high pressure”, *Mater. Sci. Eng. A*, **279** (2000) 275–281.
  24. A. Mukhopadhyay, G.B. Raju, B. Basu, “Understanding influence of  $MoSi_2$  addition (5 weight percent) on tribological properties of  $TiB_2$ ”, *Metall. Mater. Trans. A*, **39** (2008) 2998–3013.
  25. G.B. Raju, A. Mukhopadhyay, K. Biswas, B. Basu, “Densification and high-temperature mechanical properties of hot pressed  $TiB_2$ -(0–10 wt.%)  $MoSi_2$  composites”, *Scr. Mater.*, **61** (2009) 674–677.
  26. G.B. Raju, B. Basu, A.K. Suri, “Thermal and electrical properties of  $TiB_2$ - $MoSi_2$ ”, *Int. J. Refract. Met. Hard Mater.*, **28** (2010) 174–179.
  27. T.S.R.C. Murthy, J.K. Sonber, C. Subramanian, R.K. Fotedar, S. Kumar, M.R. Gonal, A.K. Suri, “A new  $TiB_2$ + $CrSi_2$  composite – Densification, characterization and oxidation studies”, *Int. J. Refract. Met. Hard Mater.*, **28** (2010) 529–540.
  28. T. Watanabe, K. Shoubu, “Mechanical properties of hot-pressed  $TiB_2$ - $ZrO_2$  composites”, *J. Am. Ceram. Soc.*, **68** (1985) C34–C36.
  29. T. Dasgupta, J. Etourneau, B. Chevalier, S.F. Matar, A.M. Umarji, “Structural, thermal, and electrical properties of  $CrSi_2$ ”, *J. Appl. Phys.*, **103** (2008) 113516.
  30. S. Lay, J.-M. Missiaen, “Microstructure and morphology of hardmetals”, pp. 91–120 in: *Comprehensive Hard Materials*. Eds. V.K. Sarin, D. Mari, L. Llanes, C. Nebel. Elsevier, 2014.
  31. A. Rabiezadeh, A.M. Hadian, A. Ataie, “Synthesis and sintering of  $TiB_2$  nanoparticles”, *Ceram. Int.*, **40** (2014) 15775–15782.
  32. Z. Fu, R. Koc, “Microstructure and mechanical properties of hot pressed submicron  $TiB_2$  powders”, *Ceram. Int.*, **44** (2018) 9995–9999.
  33. Z. Chlup, L. Baca, M. Halasova, E. Neubauer, H. Hadraba, N. Stelzer, P. Roupcová, “Effect of metallic dopants on the microstructure and mechanical properties of  $TiB_2$ ”, *J. Eur. Ceram. Soc.*, **35** (2015) 2745–2754.
  34. Atomic and Ionic Radius, <https://chem.libretexts.org/@go/page/98634>.
  35. L. Silvestroni, H.-J. Kleebe, S. Lauterbach, M. Müller, D. Sciti, “Transmission electron microscopy on Zr- and Hf-borides with  $MoSi_2$  addition: Densification mechanisms”, *J. Mater. Res.*, **25** (2010) 828–834.
  36. L. Silvestroni, S. Failla, I. Neshpor, O. Grigoriev, “Method to improve the oxidation resistance of  $ZrB_2$ -based ceramics for reusable space systems”, *J. Eur. Ceram. Soc.*, **38** (2018) 2467–2476.
  37. T.S.R.Ch. Murthy, R. Balasubramaniam, B. Basu, A.K. Suri, M.N. Mungole, “Oxidation of monolithic  $TiB_2$  and  $TiB_2$ -20wt.%  $MoSi_2$  composite at 850 °C”, *J. Eur. Ceram. Soc.*, **26** (2006) 187–192.
  38. M. Singh, H. Wiedemeier, “Chemical interactions in diboride-reinforced oxide-matrix composites”, *J. Am. Ceram. Soc.*, **74** (1991) 724–727.
  39. G.B. Raju, B. Basu, A.K. Suri, “Oxidation kinetics and mechanisms of hot-pressed  $TiB_2$ - $MoSi_2$  composites”, *J. Am. Ceram. Soc.*, **91** (2008) 3320–3327.
  40. T.S.R.Ch. Murthy, J.K. Sonber, K. Sairam, R.D. Bedse, J.K. Chakarvarty, “Development of refractory and rare earth metal borides & carbides for high temperature applications”, *Mater. Today Proc.*, **3** (2016) 3104–3113.
  41. K. Young-Hag, L. Seung-Yong, K. Hyoun-Ee, “Oxidation behavior of titanium boride at elevated temperatures”, *J. Ceram. Soc. Jpn.*, **104** (2001) 785–787.
  42. H.T. Liu, J. Zou, D.W. Ni, J.X. Liu, G.J. Zhang, “Anisotropy oxidation of textured  $ZrB_2$ - $MoSi_2$  ceramics”, *J. Eur. Ceram. Soc.*, **32** (2012) 3469–3476.